JOINT INSTITUTE FOR NUCLEAR RESEARCH

Dzhelepov Laboratory of Nuclear Problems

FINAL REPORT ON THE START PROGRAMME

Time-gated analysis in Time-Domain Diffuse Optics using Silicon Photomultipliers

Supervisor: Dr. Nikolay Anfimov

Student: Baloyi M Magezi, South Africa,
University of Pretoria

Participation Period: 13 July - 6 September,
Summer Session 2025

Dubna, 2025

Contents

Abstract

This study explores the use of Silicon Photomultipliers (SiPMs) in Time-Domain Diffuse Optics (TD-DO) for the non-invasive quantification of biological tissue oxygenation. Leveraging the high sensitivity and timing resolution of SiPMs, we demonstrate improved accuracy and sensitivity in reconstructing oxygenation levels within tissue-mimicking phantoms. The proposed method combines TD-DO with Monte Carlo inversion techniques, Time-Correlated Single Photon Counting (TCSPC), and Distribution of Time-of-Flight (DTOF) measurements. This approach holds significant promise for clinical applications, particularly in the real-time monitoring of cerebral oxygenation, thereby advancing our understanding of tissue oximetry in health and disease.

Keywords: Oxygenation, Diffuse Optics, Spectroscopy, Monte Carlo, Cerebral, Time-Domain, Silicon Photomultipliers, Tissue Oximetry

Abbreviations

ADC : Analog to Digital Converter
CW-DO : Continuous-Wave Diffuse Optics
DE : Diffusion Equation
DOS : Diffuse Optical Spectroscopy
DTOF : Distribution of Time of Flight
FD-DO : Frequency-Domain Diffuse Optics
fNIRS : Functional Near Infrared Spectroscopy
HHb : Deoxy-Haemoglobin
IRF : Instrument Response Function
LEDs : Light Emmiting Diodes
MC : Monte Carlo
MCP-PMT : Microchannel-Plate Photomultiplier tube
MRI : Magnetic Resonance Imaging
NIR : Near Infrared
NIRS : Near Infrared Spectroscopy
O_2Hb : Oxy-Haemoglobin
PTFE : PolyTetrafluoroEthylene
RTE : Radiative Transfer Equation
SC : Supercontinuum (Laser)
SiPM : Silicon Photomultiplier
SPAD : Single Photon Avalanche Diode
TAC : Time to Analog Converter
TCSPC : Time-Correlated Single Photon Counting
TDC : Time to Digital Converter
TD-DO : Time-Domain Diffuse Optics

Chapter 1

Overview on Time-Domain Diffuse Optics

1.1 Introduction

Light transmission in biological tissue is governed by absorption (μ_a) and reduced scattering ($\mu_s^{'}$). Key absorbers include oxy- and deoxy-haemoglobin (O_2Hb, HHb) and lipids, while structures such as collagen primarily drive scattering through refractive-index fluctuations at microscopic scales [1]. In the UV–visible range, absorption is strong and penetration is shallow; within the first NIR/therapeutic window ($\approx$650–950 nm), absorption decreases and scattering dominates, so photons undergo multiple scattering and diffusive transport. This transparency enabled near-infrared spectroscopy (NIRS) for non-invasive monitoring of internal physiology [2]. In time-domain diffuse optics (TD-DO), short (picosecond) pulses are launched and detected to form the distribution of time-of-flight (DTOF). The DTOF is delayed, broadened and attenuated by tissue properties; after accounting for the instrument response function (IRF) via time-correlated single photon counting (TCSPC) or fast time-to-digital conversion, its early-time shape and width are predominantly sensitive to ($\mu_s^{'}$), whereas the late-time slope reflects μ_a [3]. By exploiting early/late gates or DTOF moments, TD-DO separates scattering from absorption, increases sensitivity to deeper inhomogeneities, and reduces superficial biases (e.g skin melanin). Recent advances in silicon photomultipliers (SiPMs) have catalysed TD-DO outside specialised labs. SiPMs offer compact, low-voltage operation, high photon-detection efficiency with usable response in the NIR, sub-nanosecond timing, large dynamic range and natural scalability to multi-channel arrays—at a fraction of the size and cost of photomultiplier tubes. While higher dark-count rates, optical crosstalk and temperature dependence are practical considerations, modern devices and thermal control electronics mitigate these issues [4]. This START work investigates the use of SiPMs in TD-DO, quantifying performance trade-offs (timing jitter, PDE, dynamic range, noise) and demonstrating how SiPM-based detectors enable portable, cost-effective, and depth-sensitive NIRS measurements.

1.2 Diffuse Optics Spectroscopy (DOS)

This is a non-invasive optical technique that investigates the composition and functional state of biological tissue by analyzing how near-infrared (NIR) light propagates through it [5]. Photons are deflected by scattering events and annihilated by absorption events. The absorption and scattering processes are defined by their probability per unit distance travelled by the photon, as expressed by the absorption μ_a and scattering μ_s. The scattering process is further defined by the probability density of scattering as a function of the angle θ between the directions of scattered and incident photons, the so-called phase function p(θ) [6]. In the case of highly scattering media, where $\mu_s \gg \mu_a$, what matters is the mean cosine of the scattering angle, g=cos(θ), and a key optical parameter is the reduced scattering coefficient, $\mu_s^{'}$=μ_s(1-g), which may be interpreted as the inverse distance over which photons lose memory of their initial direction of propagation. In diffuse optics, the light distribution in tissue is described in terms of the fluence rate (ϕ), which represents the optical energy that flows per unit time per unit area along all possible directions at a given position **r** and time **t**. Diffusion theory provides an analytical description of the fluence rate through the diffusion equation:

$$\frac{\partial \phi(r,t)}{\partial t} = \nabla \cdot [D \nabla \phi(r,t)] - c\mu_a \phi(r,t) + cS_0(r,t) \tag{1.1}$$

where c is the speed of light in the medium, D=c/[3($\mu_s^{'}$+μ_a)] is the optical diffusion coefficient, and S_0 is a spherically symmetric source term [6].

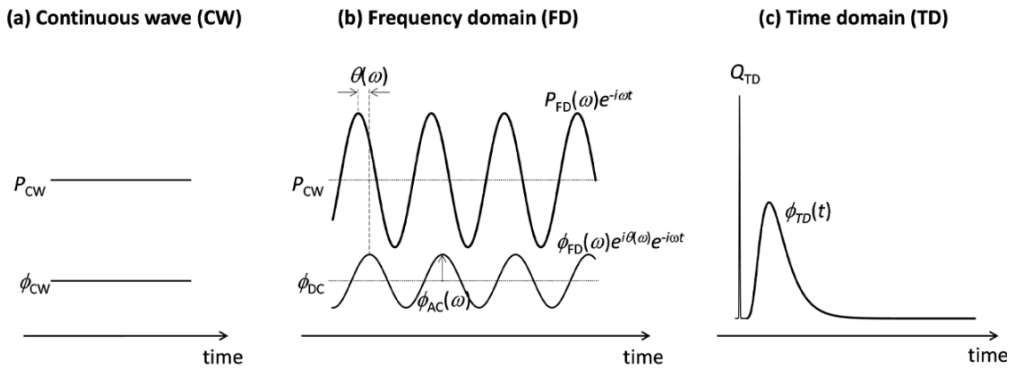

Figure 1.1: Classification of Diffuse Optical Techniques.

Diffuse optical techniques are categorized by three broad classes defined by their illumination timing: Continuous wave (CW) (constant source emission), Frequency domain (FD) (modulated source emission), and Time domain (TD) (pulsed source emission) [6]. By measuring light attenuation, phase shift, or photon arrival-time distributions at multiple wavelengths, DOS separates absorption and scattering effects [7]. The relationship between light propagation and tissue optical properties

is described using the radiative transfer equation (RTE), often simplified to the diffusion approximation for highly scattering media. In neuroscience, it is widely used to assess cerebral oxygenation, detect hypoxia, and guide interventions during surgery, anesthesia, and neonatal care [8, 9].

1.2.1 Continuous-Wave Diffuse Optics (CW-DO)

This is the simplest and most widely used approach in biomedical optics, relying on LEDs or laser diodes to deliver a steady, uninterrupted light source with constant power (P) into biological tissue [10, 11]. Because of its straightforward design and low cost, it underpins many clinical and research tools, including functional near-infrared spectroscopy (fNIRS) for monitoring brain activity [12]. The strength of this method lies in its simplicity and accessibility, allowing for portable and user-friendly devices. However, its main limitation is the absence of depth resolution, which restricts the ability to localize signals within layered tissues. As a result, continuous wave systems are often considered semi-quantitative, best suited for tracking relative changes rather than providing absolute optical measurements [13].

The fluence rate resulting from a point source embedded in a homogeneous, infinite medium depends only on the distance (r) from the source, as given by the CW solution to Eq. (1.1)

$$\phi(r) = \left(\frac{cP}{4\pi D}\right)\left(\frac{e^{-\mu_{eff}}}{r}\right) \tag{1.2}$$

where

$$\mu_{eff} = \sqrt{3\mu_a\left(\mu_s' + \mu_a\right)} \tag{1.3}$$

is the effective attenuation coefficient. Differentiation of Eq. (1.2) with respect to μ_a yields a relationship between a change in absorption and a change in the fluence rate that is referred to as the modified Beer-Lambert law [6]:

$$\Delta\mu_a = -\frac{1}{rD\,PF}\left(\frac{\Delta\phi_{cw}}{\phi_{cw}}\right) \tag{1.4}$$

where the DPF, or differential pathlength factor, is given by:

$$\mathrm{DPF}_{inf} = \frac{\sqrt{3\,\mu_s'}}{2\sqrt{\mu_a}} \tag{1.5}$$

in the infinite geometry represented by Eq. (1.2), and by:

$$\mathrm{DPF}_{seminf} = \frac{r\,\mu_{\mathrm{eff}}^2}{2\,\mu_a\left(1 + r\,\mu_{\mathrm{eff}}\right)} \tag{1.6}$$

in a semi-infinite geometry with source and detector (separated by distance r) located on the plane boundary of the medium. Equation (1.4) is widely used in CW spectroscopy of tissue [6].

1.2.2 Frequency-Domain Diffuse Optics (FD-DO)

In frequency-domain (FD) techniques, the light source emits power that is sinusoidally, amplitude-modulated at some frequency, typically laser diodes, emit light at specific wavelengths, such as 690 nm and 830 nm, into the tissue at frequencies ranging from tens to hundreds of megahertz [13]. Measurements are taken by detectors, often photomultiplier tubes or avalanche photodiodes, which capture the amplitude and phase shift of the modulated light after it has interacted with the tissue. The information content of the measured signal includes both absorption and scattering properties of the tissue, which can be quantified using the diffusion equation. Sensitivity and accuracy of these systems are enhanced by the ability to separate absorption and scattering effects, allowing for more precise estimation of tissue properties [11]. Instrumentation for frequency-domain diffuse optics typically consists of multiple source-detector pairs and complex electronics for modulation and demodulation, with some systems being designed for specific applications like breast cancer detection or brain imaging. However, limitations include complexity and cost of the instrumentation, as well as potential limitations in depth penetration and spatial resolution. Despite these limitations, frequency domain diffuse optics-based systems also offer a powerful tool for non-invasive tissue assessment [13].

$$\phi(r,\omega) = \frac{cP(\omega)}{4\pi D}\,\frac{e^{-r\mu_{\text{eff}}\sqrt{1-i\frac{\omega}{c\mu_a}}}}{r} \tag{1.7}$$

The fluence rate of Eq. (1.7) should be interpreted as the complex amplitude of a sinusoidal oscillation at frequency ω associated with an implied sinusoidal factor $e^{-i\omega t}$. Such complex amplitude represents the magnitude and the phase of the oscillatory fluence rate that is measured in the FD-NIRS [6].

1.2.3 Time-Domain Diffuse Optics (TD-DO)

Time-Domain Diffuse Optics (TD-DO) is an advanced photonic technique that involves the injection of ultrashort pulses of near-infrared (NIR) light typically with durations on the order of tens to hundreds of picoseconds into highly scattering media, such as biological tissues, to investigate their internal optical properties [14]. In essence, TD-DO operates by tracking the distribution of time-of-flight (DTOF) of photons that have undergone multiple scattering and absorption events within the medium before re-emerging and being detected by the (SiPM) at the surface. Unlike continuous-wave (CW) or frequency-domain (FD) approaches, TD-DO captures the full temporal profile of the transmitted or reflected light pulse, enabling a time-resolved measurement that can separate the effects of absorption and scattering with high precision [13]. The key principle is that photons traveling longer, more scattered paths arrive later at the detector, and are more likely to have penetrated deeper into the medium, while early-arriving photons represent more superficial interactions, this can be observed using a technique called time-correlated single photon counting (TCSPC). From a theoretical standpoint, the photon propagation is modeled using the radiative transfer equation (RTE), though due to its computational complexity, the diffusion equation (DE) is typically used as a practical approximation in highly scattering media. The temporal broadening, delay, and attenuation of the detected light pulse are directly related to the tissue's optical absorption coefficient (μ_a) and reduced scattering coefficient (μ_s), which TD-DO can quantitatively retrieve through inverse modeling techniques [7].

$$\phi(r,t) = \frac{Qc}{(4\pi Dt)^{3/2}}\exp\!\left(-\frac{3r^2}{4Dt}\right) - \mu_a\, ct \tag{1.8}$$

The TD fluence rate of Eq. (1.8) is representative of the photon time-of-flight distribution [6].

1.3 Photon Detectors

1.3.1 Microchannel-plate Photomultipliers (MCP-PMT)

Microchannel-plate photomultiplier tubes (MCP-PMT) are vacuum photodetectors that couple a photocathode to one or more microchannel plates. A photon liberates a photoelectron at the photocathode; an extraction field accelerates it into a tilted glass capillary (pore $\approx$ 6–25 μm, aspect ratio 40:1) held at high bias. Repeated wall impacts generate secondary electrons, yielding avalanche gain of $10^5 - 10^7$ [15]. One or two MCPs (chevron/Z-stack) feed a fast anode (single, multi-anode, or delay-line), producing sub-nanosecond pulses with transit-time spread $\approx$ 20–50 ps FWHM and spatial resolution set by pore size and anode segmentation [16]. These traits make MCP-PMT a benchmark for ultrafast photon counting in Cherenkov imaging, time-resolved spectroscopy, and FLIM. Practical constraints include lower quantum efficiency in the NIR for common photocathodes, gain saturation at high local rates, photocathode ageing from ion feedback (mitigated by ALD-coated MCPs), and the need for kilovolt-level bias and vacuum packaging. Relative to SiPM, MCP-PMT offer superior single-photon timing, whereas SiPM provide low-voltage operation, robustness, scalable arrays, and strong NIR performance—key trade-offs when selecting detectors for time-domain diffuse optics [8].

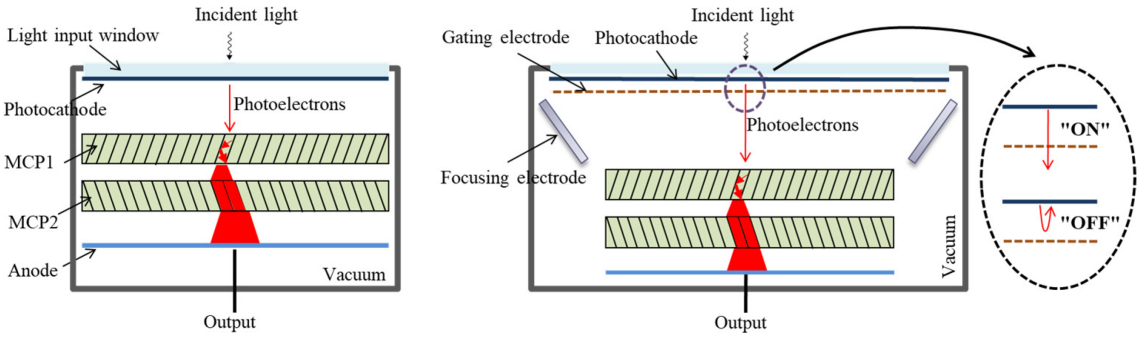

(a) The conventional MCP-PMT (b) The large area MCP-PMT with gating function

Figure 1.2: Schematic diagram of typical Microchannel-plate Photomultiplier tubes (MCP-PMT).

1.3.2 Silicon Photomultiplier (SiPM)

Silicon Photomultipliers (SiPM), As shown on (Fig. 1.3) are compact solid-state photodetectors that combine single-photon sensitivity with sub-nanosecond timing resolution. Structurally, they consist of an array of avalanche photodiode (APD) microcells operated in Geiger mode and connected in parallel on a common silicon substrate [15]. When an incident photon is absorbed, it generates an

electron–hole pair that is accelerated by a strong external electric field. Through impact ionization, a self-sustaining avalanche is triggered, producing a digital output pulse from the microcell [17]. A built-in quenching resistor then halts the avalanche, after which the microcell recharges and becomes ready to detect another photon. The collective summation of signals from thousands of such microcells yields an output proportional to the number of detected photons, enabling both single-photon counting and intensity measurements [17]. They operate on low voltage, insensitive to magnetic fields, and scalable integration. These features make SiPM highly attractive for applications ranging from medical imaging (e.g PET scanners) and high-energy physics (e.g Scintillation detectors) to astrophysics, quantum technologies, and optical communications. Their ongoing development, focused on reducing dark count rates, optical crosstalk, and afterpulsing while extending near-infrared sensitivity, continues to expand the role of SiPM as a versatile detector technology in both fundamental research and applied sciences [15].

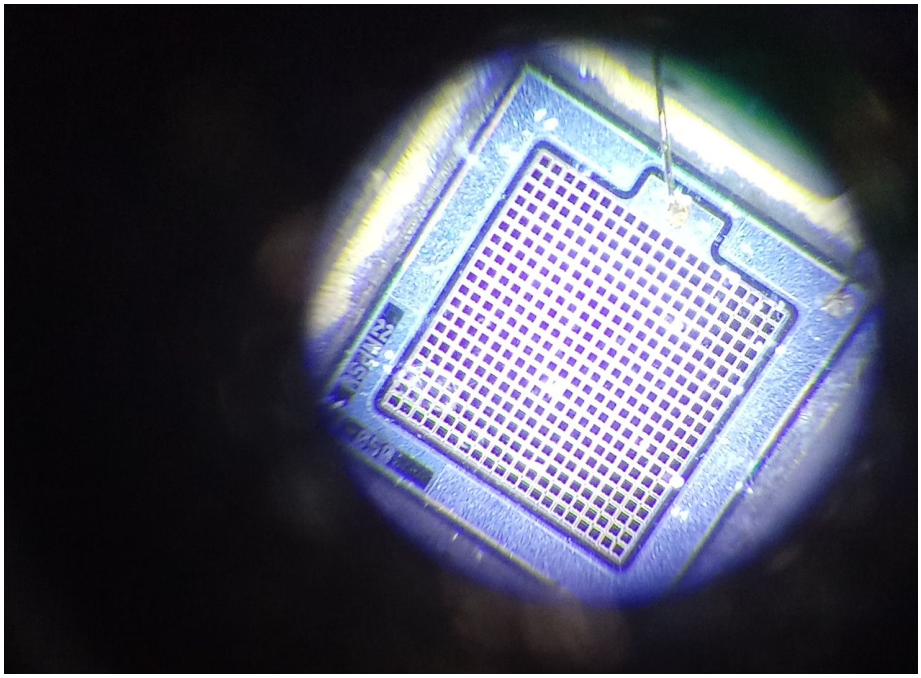

Figure 1.3: Hamamatsu (S13369-6050CS) model Silicon Photomultiplier (SiPM).

SiPMs are characterized by several key advantages over traditional photomultiplier tubes, making them highly suitable for time-domain diffuse optics. These solid-state detectors offer high internal gain (10^5–10^6), single-photon sensitivity, and excellent photon detection efficiency (PDE $> 20\%$). Furthermore, they provide superior performance in a compact and robust package, featuring fast timing resolution (< 100 ps) for precise time-of-flight measurement and low dark count rates to maintain a high signal-to-noise ratio [18].

Chapter 2

Oximetry of deep tissues

2.1 Principle of Oximetry with TD-DO

Time-domain diffuse optics (TD-DO) measures deep-tissue oximetry by launching picosecond light pulses and recording the temporal point-spread function/ distribution of time-of-flight (TPSF/DTOF) a histogram of photon arrival times at a fixed source–detector separation [18]. The DTOF is modelled with a solution of the diffusion equation for an appropriate geometry (e.g semi-infinite, slab, or two-layer scalp/brain), and critically this model is convolved with the instrument response function (IRF) to account for laser pulse width, fibre/optics broadening, and detector timing jitter; explicit deconvolution is generally avoided because it is numerically unstable. Fitting (e.g via Levenberg–Marquardt minimising reduced χ^2) is performed over a robust temporal window typically from around 90% of the peak on the rising edge to ≈1% of the peak on the late tail—to exclude pre-diffusive times while retaining the late photons that probe deeper tissue [16]. From the fit, one retrieves the absorption (μ_a) and reduced scattering (μ_s') spectra; because late-time DTOF slope is dominated by μ_a and the early width/shape by μ_s' (after IRF), TD-DO naturally separates absorption from scattering. Multi-wavelength measurements then convert $\mu_a(\lambda)$ into chromophore concentrations by solving:

$$\mu_a(\lambda) \approx \varepsilon_{\mathrm{O_2Hb}}(\lambda)[\mathrm{O_2Hb}] + \varepsilon_{\mathrm{HHb}}(\lambda)[\mathrm{HHb}]$$

, yielding [O_2Hb] and [HHb] and thus tissue oxygen saturation:

$$StO_2 = \frac{[O_2Hb]}{[O_2Hb] + [HHb]} \times 100\%$$

Late-gate analyses and two-layer models increase sensitivity to cerebral (or otherwise deep) regions while reducing superficial bias. Silicon photomultiplier (SiPM), operated in Geiger mode and read out by TCSPC/TDC electronics, provide single-photon sensitivity with sub-nanosecond timing, enabling precise DTOF recording; care is taken when fitting an additional temporal offset to correct for instrumental drift, as this can introduce parameter crosstalk. Together, these steps deliver quantitative, depth-weighted oximetry of deep tissues in a non-invasive manner [19].

2.2 Advantages and challenges

Time-domain diffuse optics (TD-DO) launches picosecond pulses and analyses the distribution of time-of-flight (DTOF) of detected photons to separate absorption (μ_a) from reduced scattering ($\mu_s^{'}$) and to weight sensitivity toward deeper layers via late-time photons [16]. A forward model (diffusion or Monte Carlo for a chosen geometry) is involved with the instrument response function (IRF) and fitted (e.g reduced χ^2 over a robust temporal window that excludes pre-diffusive times and noisy tails) to retrieve μ_a and $\mu_s^{'}$. DTOF moments can provide fast, stable estimates. Multi-wavelength $\mu_a(\lambda)$ then yields [O_2Hb], [HHb], and StO_2, with reduced superficial bias compared with CW [19]. Practical limits include the photon-economy trade-off (late gates have poor SNR), IRF stability and timing drift, TCSPC pile-up/dead time, and detector effects (SiPM dark counts/crosstalk, jitter), plus motion and coupling artifacts in vivo. Careful calibration with phantoms, thermal control, and modern GPU-accelerated Monte Carlo mitigate many of these issues, enabling quantitative, depth-weighted oximetry [20].

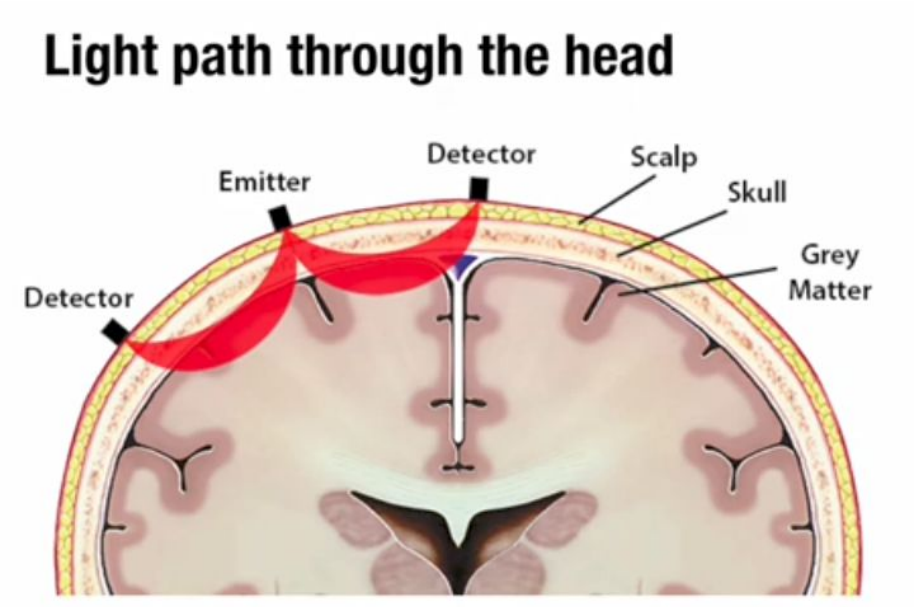

Figure 2.1: Visualization of photon propagation through the layered structure of the human head during diffuse optical imaging (DOI).

A light source emits near-infrared photons onto the scalp, and the photons propagate through various biological layers before reaching a detector placed at a fixed distance. (see Fig. 2.1), The light path shown by the red heatmap curves) follows a banana-shaped trajectory, representing the typical photon migration route in time-domain diffuse optics (TD-DO). As photons travel through the tissue, they undergo multiple scattering events, allowing them to penetrate and sample deeper layers of the brain [20].

Chapter 3

Experimental Setup and Methods

3.1 Purpose of the Study

3.1.1 Aim

This study was aimed to investigate the timing information acquired with the light source-detector system using the tissue mimicking phantom prototype for medical applications.

3.1.2 Objectives

- Participation in measurements of a tissue-mimicking phantom with well-defined optical properties to serve as a calibrated test platform.
- Use DLNP time-domain scanning system to acquire single-photon time-of-flight (DTOF) distributions across the phantom surface.
- Process the time-resolved data to plot the scanning map.
- Analyze the data by comparing the DTOFs and time-gated signals.

3.2 Setup

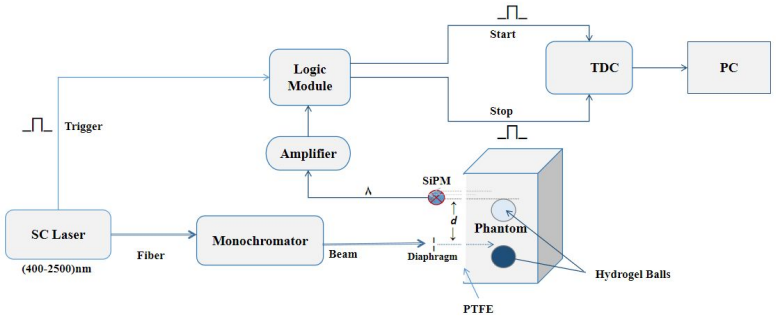

Figure 3.1: Schematic of the custom time-domain diffuse optics (TD-DO) setup.

As illustrated on (Fig. 3.1), A supercontinuum laser and monochromator provide tunable wavelength input to a tissue-like phantom, while a SiPM and time-to-digital converter (TDC) resolve the resulting temporal photon distribution for time-correlated spectroscopy.

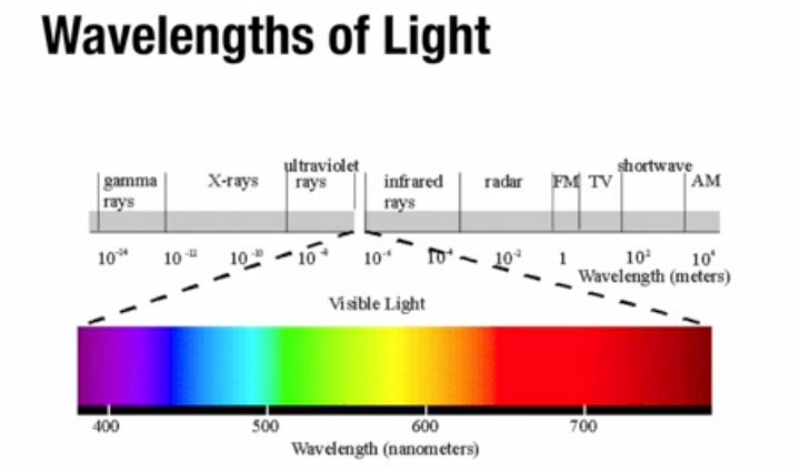

Figure 3.2: The Electromagnetic (EM) spectrum.

Biological tissue becomes semi-transparent in a specific near-infrared "optical window" (see Fig. 3.2), allowing light to penetrate deep into the body and act as an X-ray for blood oxygen and composition.

3.2.1 Materials (Phantom)

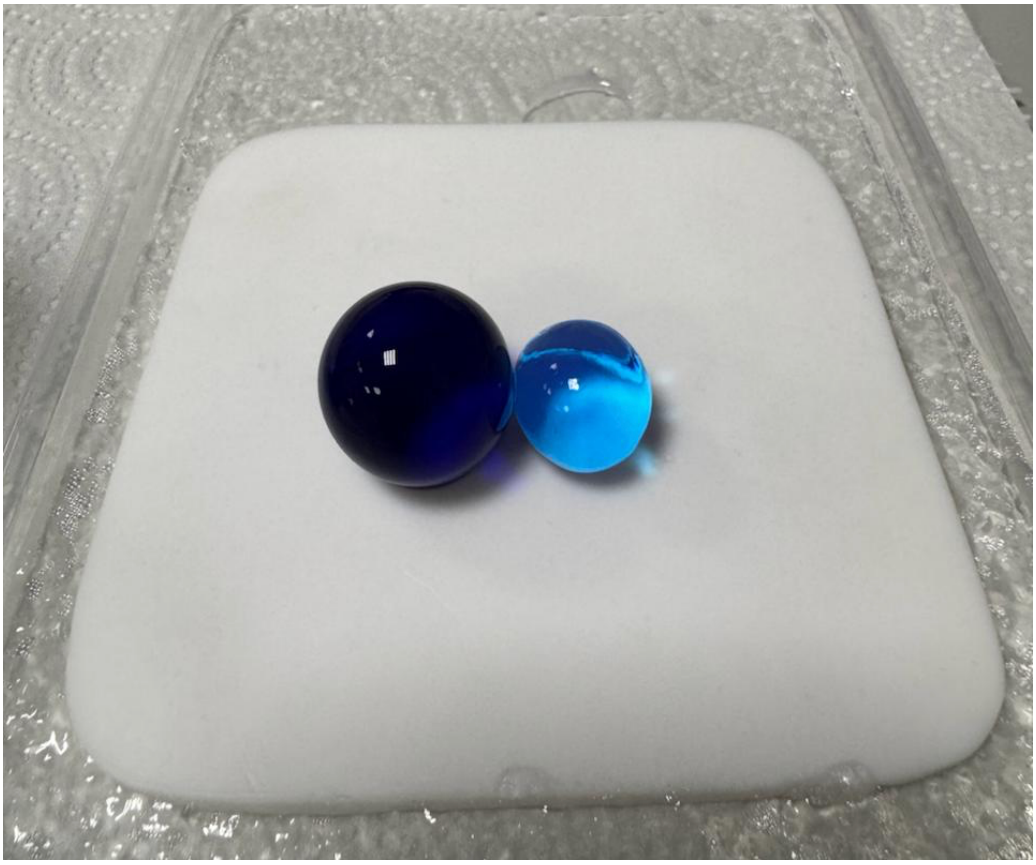

Figure 3.3: Simulation of affected and healthy tissue regions using hydrogel spheres.

The dark blue sphere (stained with methylene blue) represents an infected region, and it is characterized by restricted diffusion and cell death. The light blue (water-filled sphere) illustrates a healthy tissue with normal blood perfusion. (see Fig. 3.3) The contrast between the two models placed on top of the PTFE highlights the structural and biochemical differences observed between damaged and unaffected tissue areas.

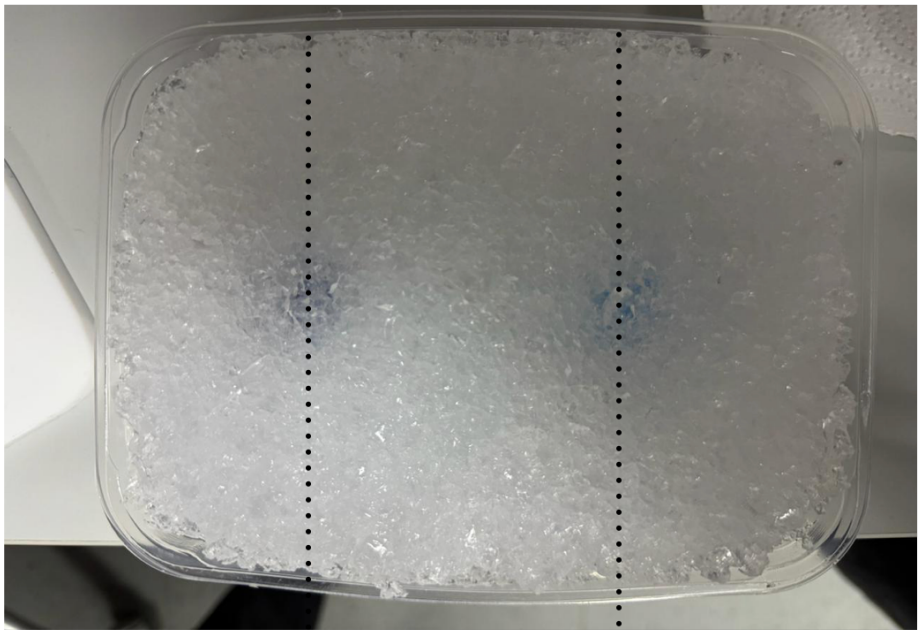

Figure 3.4: Tissue-simulating phantom with spherical inclusions.

A tissue-simulating phantom was fabricated from a hydrogel-base, silicon dioxide (RH-SIL-400) scatterer, and methylene blue absorber. Two 2 cm hydrogel spherical inclusions were embedded (see Fig. 3.4) at equidistant positions within the scattering medium to mimic the structural heterogeneity of stroke-affected brain tissue. This configuration provides a controlled platform for quantifying light absorption, scattering, and diffusion contrast between healthy and pathological regions.

3.3 Procedure

The supercontinuum (SC) laser source (400–2500 nm) was triggered to generate broadband pulsed light, which was delivered through an optical fiber into a monochromator for wavelength selection. The output beam was shaped by a diaphragm and directed onto the tissue-equivalent phantom. Photons emerging from the phantom were detected by a silicon photomultiplier (SiPM), and the resulting signals were amplified by the amplifier and shaped by a logic module. The laser trigger provided a start signal, while photon detection produced a stop signal, both of which were processed by the GP22 time-to-digital converter (TDC) to measure photon time-of-flight. The recorded data were transferred to a computer, where histograms of photon arrival times were constructed using time-correlated single photon counting (TCSPC). Diffusion-based models were fitted to the histograms to extract the absorption and reduced scattering coefficients of the phantom. Measurements were repeated for wavelengths ranging from (650,700,750 to 800) nm selected by the monochromator respectively, to obtain wavelength-dependent optical properties. Throughout the procedure, the SiPM was shielded from ambient light as the experiment took place in the dark room, and optical power levels were monitored to ensure safe and reliable operation.

Chapter 4

Results and Discussions

4.1 Time resolution requirements

The reconstruction of the photon time-of-flight distribution in (TD-DO) was achieved through (TC-SPC). In this technique, individual photon arrival times were recorded with respect to a trigger signal provided by the periodic laser cycle, and the accumulated time-stamps are used to build histograms of photon arrival times [21]. The timing electronics required for this process are typically based either on a combination of a time-to-analog converter (TAC) and an analog-to-digital converter (ADC), or on a time-to-digital converter (TDC). In the first case, the difference between the start and stop signals is converted into an analog voltage, which is subsequently digitized by the ADC [16]. In the second case, the delay was directly converted into a digital code. Systems employing TAC–ADC architectures are generally characterized by superior timing resolution and linearity, although they are more costly and less easily integrated.
In contrast, TDC-based systems can be integrated into a single chip and are therefore better suited for multi-channel implementations, albeit with poorer timing performance and reduced sustainable count rates [19]. The overall time resolution in TD-DO was not determined solely by the electronics but also by the instrument response function (IRF), which is defined by the convolution of the laser pulse width, detector jitter, and electronic jitter. Ultrafast laser pulses (typically between 50 and 100 ps) were required to ensure adequate temporal precision. Detector contributions, particularly the timing jitter of photomultiplier tubes, avalanche photodiodes, or silicon photomultipliers, also play a significant role in defining the achievable resolution [22, 23]. To accurately resolve absorption and scattering changes in biological tissue, a system IRF with a full width at half maximum (FWHM) of approximately 100 ps or better is typically required. Considerations of throughput, dead-time, and pile-up effects must also be included to ensure reliable measurements [20].

4.1.1 Analysis of Late-Time Photon Counts

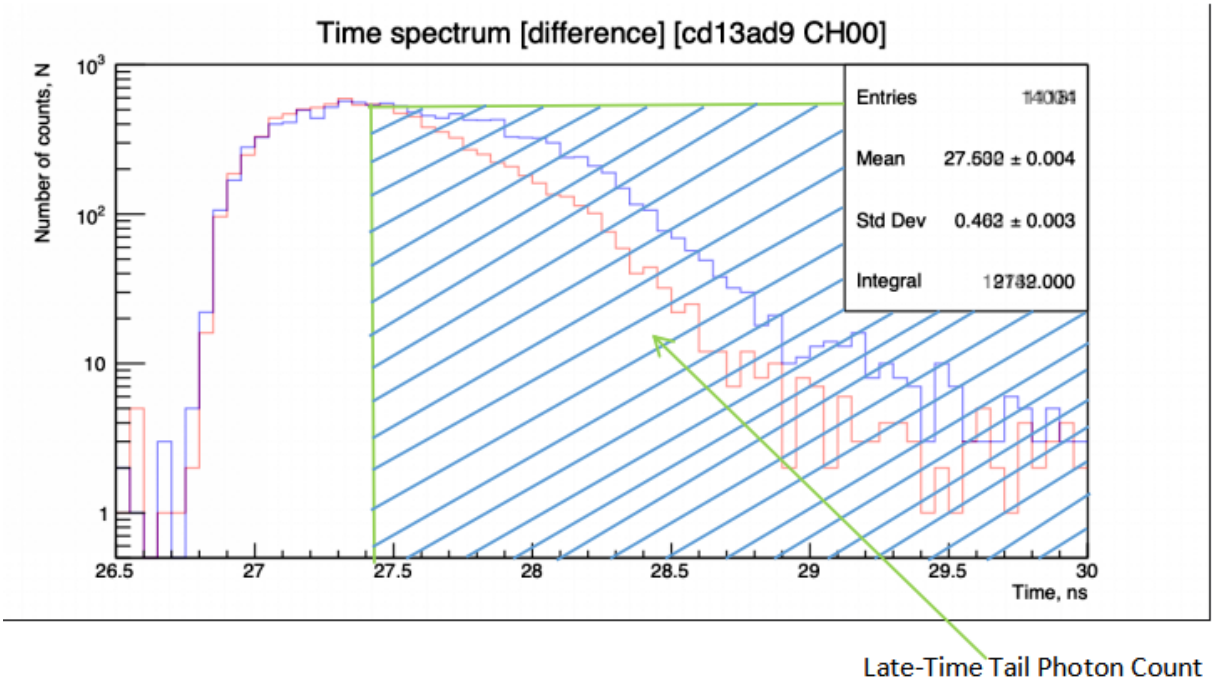

Figure 4.1: Comparison of Temporal distribution of photons on a logarithmic scale.

The right-shift of the red DTOF curve from (Fig. 4.1 above) indicates a clear increase in the reduced scattering coefficient ($\mu_s^{'}$) of the phantom hydrogel. This was not a mere change in phantom condition but it was as a result of immersing the one Hydrogel in methylene blue and another in pure water . The data shows that embedding the photon-hydrogel balls to mimic de oxygenation fundamentally altered the material's scattering properties. The balls introduced additional, efficient absorbing centers, increasing the average photon path length and delaying their time-of-flight. The prototype successfully mimicked a key aspect of hypoxic or affected tissue—increased light absorption, likely analogous to cellular swelling (edema) or structural change. The measurement demonstrates high sensitivity to this microscopic biological perturbation, which is a more profound biomarker than a mere change in blood color.

4.1.2 Spatial Mapping of Optical Properties.

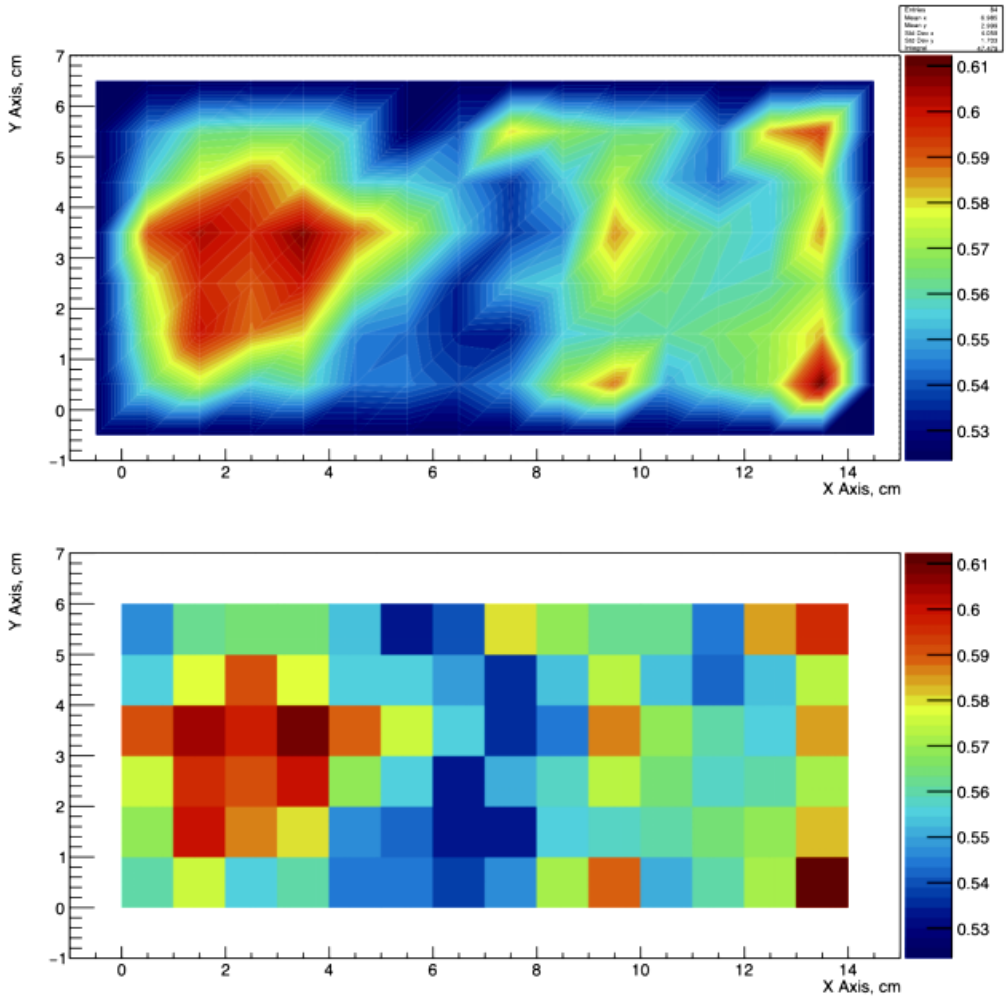

Figure 4.2: The phantom reconstruction using time-gated algorithm.

Time-Gated ratio algorithm (see Fig. 4.2) identifying non-uniformity region by mapping the tail-to-total photon ratio computing the value:

$$R = \frac{N_{\text{tail}}}{N_{\text{total}}} \tag{4.1}$$

For that specific point, creating a visual contrast that highlights areas of altered optical response. A color gradient was used to visually represent the numerical ratio values, with warmer colors (e.g red, yellow) indicating higher values and cooler colors (e.g blue, green) indicating lower values,

as defined by a quantitative colorbar legend. On Fig. 4.2 (Top) an interpolated map provides a smoother, higher-resolution visualization by estimating data between points, making changes easier to see, while a non-interpolated map shown on Fig. 4.2 (Bottom) shows the raw, discrete data points, preserving original measurements at the cost of lower spatial resolution.

4.2 Conclusions

This START project successfully achieved its aim of investigating timing information for medical applications by developing and validating a complete experimental setup for time-domain diffuse optics. The core objective was met through the creation of a tissue-mimicking phantom prototype and a complex data acquisition system using a supercontinuum laser, monochromator, and silicon photomultiplier (SiPM) detector. The system effectively acquired single-photon time-of-flight (DTOF) distributions at wavelengths (650–800 nm) using Time-Correlated Single Photon Counting (TCSPC) methodology. Key performance factors, including the instrument response function (IRF) and the trade-offs on TDC timing electronics, were central to achieving the precise temporal resolution necessary for resolving tissue optical properties.
Analysis of the recorded histograms confirmed the system's capability to extract accurate absorption and reduced scattering coefficients by fitting diffusion-based models to the data. Furthermore, the application of the Time-Gated ratio algorithm demonstrated a powerful method for identifying and visualizing regions of altered optical response, such as strokes. This was illustrated by comparing interpolated maps, which offer high-resolution visualization for clinical interpretation, with non-interpolated maps, which preserve the integrity of the raw experimental data. In summary, this work establishes a robust foundation for advanced time-resolved optical measurements. It validates the prototype's functionality in quantifying wavelength-dependent optical properties and highlights its significant potential for future medical diagnostic applications, particularly in the functional imaging and detection of cerebral conditions.

4.3 Acknowledgements

I extend my sincere gratitude to my supervisor, Dr. Nikolay Anfimov and his associates, Mr. Alexander Selyunin and Mr. Vladislav Sharov for their invaluable guidance and mentorship throughout this research project. I am also deeply thankful to my supervisor at my home university Prof. M Diale, for her unwavering support and for enabling my participation in this session. This work was made possible by the generous opportunity provided by the Joint Institute for Nuclear Research (JINR) University Center to take part in this Student Advanced Research Training (START) Summer Session. Lastly I gratefully acknowledge the Dzhelepov Laboratory of Nuclear Problems (DLNP) for providing access to their exceptional facilities.

References

[1] J. Aguirre, J. Ripoll, B. Cox, S. Arridge *et al.*, "Monte carlo-based diffuse optical spectroscopy for breast cancer diagnosis," *Journal of Biomedical Optics*, vol. 18, no. 10, p. 105008, 2013.

[2] K. H. Chan *et al.*, "Broadband diffuse optical spectroscopy for non-invasive measurement of brain oxygenation," *NeuroImage*, vol. 52, no. 2, pp. 462–471, 2010.

[3] T. Durduran *et al.*, "Diffuse optical measurement of blood flow, blood oxygenation, and metabolism in a human brain during sensorimotor cortex activation," *Optics Letters*, vol. 35, no. 12, pp. 2086–2088, 2010.

[4] S. L. Ferradal *et al.*, "Functional imaging of the developing brain with diffuse optical tomography," *Journal of Neuroscience Research*, vol. 92, no. 5, pp. 579–591, 2014.

[5] Q. Fang and D. A. Boas, "Monte carlo simulation of photon migration in 3d turbid media accelerated by graphics processing units," *Optics Express*, vol. 17, no. 22, pp. 20 178–20 190, 2009.

[6] S. Fantini and A. Sassaroli, "Near-infrared optical mammography for breast cancer detection with intrinsic contrast," *Annals of Biomedical Engineering*, vol. 40, no. 2, pp. 398–407, 2012.

[7] Y. Yu, A. Sassaroli, D. K. Chen, M. J. Homer, R. A. Graham, and S. Fantini, "Near-infrared, broad-band spectral imaging of the human breast for quantitative oximetry: Applications to healthy and cancerous breasts," *Journal of Innovative Optical Health Sciences*, vol. 3, no. 3, pp. 267–277, 2010.

[8] C. Fernandez, G. Blaney, J. Frias, F. Tavakoli, A. Sassaroli, and S. Fantini, "Single-distance and dual-slope frequency-domain near-infrared spectroscopy to assess skeletal muscle hemodynamics," *Journal of Biomedical Optics*, vol. 28, no. 12, p. 125004, 2023.

[9] F. Tavakoli, C. Fernandez, G. Blaney, J. Frias, A. Sassaroli, and S. Fantini, "Muscle hemodynamics measured with dual-slope frequency-domain near-infrared spectroscopy," in *Proceedings of SPIE*, vol. 12838, 2024, p. 1283807.

[10] D. A. Boas *et al.*, "Three dimensional monte carlo code for photon migration through complex heterogeneous media including the adult human head," *Optics Express*, vol. 12, no. 14, pp. 3221–3233, 2004.

[11] A. T. Eggebrecht *et al.*, "Mapping distributed brain function and networks with diffuse optical tomography," *Nature Photonics*, vol. 8, no. 6, pp. 448–454, 2014.

[12] D. K. Chen, M. K. Erb, Y. Tong, Y. Yu, A. Sassaroli, P. R. Bergethon, and S. Fantini, "Spectral and spatial features of diffuse optical signals in response to peripheral nerve stimulation," *Biomedical Optics Express*, vol. 1, no. 3, pp. 923–942, 2010.

[13] M. K. Erb, D. K. Chen, A. Sassaroli, S. Fantini, and P. R. Bergethon, "Diffuse optical signals in response to peripheral nerve stimulation reflect skeletal muscle kinematics," *Biomedical Optics Express*, vol. 1, no. 3, pp. 943–954, 2010.

[14] Y. Hoshi *et al.*, "Quantitative measurement of muscle oxygenation using near-infrared spectroscopy," *Journal of Applied Physiology*, vol. 111, no. 4, pp. 1040–1047, 2011.

[15] C. Fernandez, T. Das, G. Blaney, Z. Haga, T. McWilliams, J. Mertens, A. Sassaroli, and S. Fantini, "Coherent spontaneous hemodynamics in the human brain," *IEEE Open Journal of Engineering in Medicine and Biology*, vol. 4, pp. 102–108, 2023.

[16] A. Pifferi *et al.*, "Time-domain diffuse optical imaging with silicon photomultipliers," *Optics Express*, vol. 27, no. 15, pp. 21 346–21 361, 2019.

[17] T. T. Pham, C. Fernandez, G. Blaney, K. Tgavalekos, A. Sassaroli, X. Cai, S. Bibu, J. Kornbluth, and S. Fantini, "Noninvasive optical measurements of dynamic cerebral autoregulation by inducing oscillatory cerebral hemodynamics," *Frontiers in Neurology*, vol. 12, p. 745987, 2021.

[18] G. Blaney, C. Fernandez, A. Sassaroli, and S. Fantini, "Dual-slope imaging of cerebral hemodynamics with frequency-domain near-infrared spectroscopy," *Neurophotonics*, vol. 10, no. 1, p. 013508, 2023.

[19] L. D. Sieno *et al.*, "Sipm-based time-domain diffuse optical tomography for brain imaging," *IEEE Transactions on Medical Imaging*, vol. 39, no. 10, pp. 3054–3064, 2020.

[20] D. Contini *et al.*, "Time-domain diffuse optical spectroscopy using silicon photomultipliers," *Optics Letters*, vol. 42, no. 19, pp. 3940–3943, 2017.

[21] A. D. Mora *et al.*, "Silicon photomultipliers for time-domain diffuse optical imaging," *Journal of Biomedical Optics*, vol. 25, no. 4, pp. 1–10, 2020.

[22] E. Martinenghi *et al.*, "Silicon photomultipliers for diffuse optical imaging," *Journal of Physics D: Applied Physics*, vol. 51, no. 30, p. 304001, 2018.

[23] A. Kalitzeos *et al.*, "Time-domain diffuse optical imaging using silicon photomultipliers," *Biomedical Optics Express*, vol. 10, no. 4, pp. 1746–1761, 2019.